Design of InAs/GaSb superlattice infrared barrier detectors

M.Delmas[1], R. Rossignol[2,3], J.B. Rodriguez[2,3], P. Christol[2,3]

[1]School of Physics and Astronomy, Cardiff University, The Parade, Cardiff CF243AA, UK
[2] Univ. Montpellier, IES, UMR 5214, F- 34000, Montpellier, France.
[3] CNRS, IES, UMR 5214, F- 34000, Montpellier, France

Abstract

Design of InAs/GaSb type-II superlattice (T2SL) infrared barrier detectors is theoretically investigated. Each part of the barrier structures is studied in order to achieve optimal device operation at 150K and 77K, in the midwave and longwave infrared domain, respectively. Whatever the spectral domain, nBp structure with a p-type absorbing zone and an n-type contact layer is found to be the most favourable detector architecture allowing a reduction of the dark-current associated with generation-recombination processes. The nBp structures are then compared to pin photodiodes. The MWIR nBp detector with 5 µm cut-off wavelength can operate up to 120K, resulting in an improvement of 20K on the operating temperature compared to the pin device. The dark-current density of the LWIR nBp device at 77K is expected to be as low as 3.5 x 10^{-4} A/cm^2 at 50 mV reverse bias, more than one decade lower than the usual T2SL photodiode. This result, for a device having cut-off wavelength at 12 µm, is at the state of the art compared to the well-known MCT 'rule 07'.

Keywords: InAs/GaSb superlattice, barrier detector, infrared detector, TCAD simulation, dark current

Highlights :

1- InAs/GaSb type-II superlattice barier detectors have been designed for the MWIR and for the LWIR

2- MWIR nBp T2SL detector can operate up to 120K

3- LWIR nBp T2SL detector can compete with well established MCT technology.

1. Introduction

High-performance photodetectors operating in the midwave (MWIR, 3 – 5 µm) and longwave (LWIR 8 – 12 µm) infrared spectral domain are useful for a broad range of applications such as civil, industrial and military. Since the proposition made by Smith and Mailhiot [**1**], the Type-II InAs/GaSb superlattice (T2SL) material has been of great interest as it offers unique properties for IR detection including a high effective mass, the reduction of Auger recombination rates and the possibility to address a wide range of wavelength from the MWIR to LWIR domain. However, the dark-current of pin photodiodes has not yet reached its theoretical predictions due to a short minority carrier lifetime ranging from 10 to 150 ns at 77K [**2**] resulting in a large generation-recombination (G-R) current that limits the electrical performances at low temperatures. Recently, the InAs/InAsSb SL (also known as the 'Ga-Free' SL) has been proposed as an alternative to the T2SL technology since a longer minority carrier lifetime has been reported both in the MWIR and LWIR spectral range [**3, 4**]. Unfortunately, until now, Ga-Free detector performances have not proved to be superior than those of T2SL detectors [**5, 6**].

Since the demonstration of barrier structures by Maimon and Wicks in 2006 [**7**], many efforts have been made by research groups to improve the device design of T2SL detectors [**8-11**] and to achieve a significantly lower dark-current, or higher operating temperature, than that of the standard pin photodiode. In a barrier structure, a large band gap material, namely the barrier layer, is inserted to block the majority carriers while allowing unimpeded transport of the minority carriers. The electric field being confined in the barrier layer, the G-R current is suppressed in the absorption region. The dark-current of such a structure, when properly designed, is thus diffusion-limited whatever the temperature. The electrical performances should, *a priori*, be improved compared to the pin photodiode. However, at high temperature, since T2SL pin photodiodes are also limited by the diffusion contribution [**12**], a lower improvement is expected in comparison with low temperatures.

The objective of this paper is to design and to theoretically evaluate, by using the commercial TCAD ATLAS software from SILVACO [**13**], the performances of T2SL barrier infrared detectors. The following section is devoted to the design of a T2SL MWIR barrier structure with a 5 µm cut-off wavelength at 77K. In this section, the composition, thickness and doping level of the absorbing, barrier and contact layers are accurately chosen. Next, the dark-currents of the selected T2SL MWIR barrier detector, for temperatures ranging from 77 up to 200K, are calculated at -50 mV and compared with those of equivalent T2SL MWIR pin photodiodes. The analysis of these results is made in term of temperature operation. Finally, a T2SL LWIR barrier device having a cut-off wavelength of 12 µm is defined and the dark-current is evaluated for a temperature of 77K.

2. Design of the MWIR T2SL barrier structure

The barrier structure is composed of a contact layer, a barrier layer and an active absorption region (n or p type) for which several engineered heterostructures can be considered such as *nBn* [**8**], *p-π-M-p* [**9**], *CBIRD* [**10**] and *pBp* [**11**]. The aim of this section is to define by simulation the composition, doping and thickness of each layer. Numerical simulations were performed using the ATLAS software, which has already been used to calculate the band diagram and the dark current of IR photodiodes [**14-16**]. In the case of MWIR T2SL structure, a bulk-based model using effective masses, band gap and density of states is considered.

2.1 Thickness and doping level of the absorption region

Firstly, the T2SL absorption region suitable for the MWIR domain has to be defined. As the material composing the active region, the p-type T2SL with 7 monolayers (ML) of InAs and 4 ML of GaSb (referred to as the 'InAs-rich SL') was chosen, since it presents the best performances in terms of dark current and quantum efficiency (QE) for a cut-off wavelength of 5 µm at 77K [**12, 17**]. To determine the absorption region thickness, QE simulations on pin photodiodes have been performed to extract the minority carrier diffusion length. The material parameters used for the simulation of the InAs-rich SL structure are summarized in **Table I** [**14**].

The LUMINOUS module integrated into ATLAS calculates the photogeneration rate in the presence of a defined beam (intensity, wavelength) that is taken into account in the generation terms of the carrier continuity equations. The quantum efficiency can then be calculated by dividing the current from one of the device electrodes by the source photo-current which can be considered as the rate of incident photons on the device. The quantum efficiency depends on two important mechanisms: the absorption by the semiconductor material and the transport of the photogenerated carriers from the absorption region to the metallic contacts where they can be collected.

On one hand, the absorption coefficient α of the InAs-rich SL has been calculated as a function of the wavelength λ using equation (1) and the imaginary part κ of the complex optical index measured and simulated on an InAs-rich structure [**18**].

$$\alpha(\lambda) = \frac{4\pi\kappa(\lambda)}{\lambda} \quad (1)$$

At 77K, the calculated absorption coefficient is equal to 2 820 cm^{-1} at 4 µm for a structure having a cut-off wavelength equal to 5 µm. Note that, this value is consistent with the experimental value measured for an equivalent InAs-rich structure [**19**].

On the other hand, the carrier transport can be described by the minority carrier lifetime τ and mobility μ which determine the diffusion length L_{diff} according to the well-known following equation (2):

$$L_{diff} = \sqrt{\frac{kT}{q}\mu.\tau} \quad (2)$$

where T is the temperature, k is the Boltzmann constant and q is the electronic charge.

The minority carrier lifetime can be extracted by simulating the dark-current density using the models and method described in a previous paper [**14**]. We found that the experimental dark-current of several InAs-rich pin photodiodes can be accurately described using a minority carrier lifetime of 100 ns which is the typical value measured for MWIR T2SL [**20, 21**].

The absorption coefficient and the minority carrier lifetime being fixed, the diffusion length is the adjustable parameter through the mobility. In the existing literature, only few experimental values for the mobility are reported [**22-24**]. Indeed, considering the anisotropy of the T2SL material, the experimental mobility is hardly interpretable due to the contribution of the mobility parallel to the growth direction and the one perpendicular. The extracted mobility for our simulation is thus difficult to compare with experimental values since in addition it strongly depends on the T2SL period composition and thickness.

The QE for two InAs-rich pin photodiodes (without considering in the simulation an antireflection coating) having different absorption thickness has been calculated and is plotted in **Figure 1**. The p-type absorption region is 500 nm and 4 µm thick for sample A and B, respectively. To obtain the curves shown in **Figure 1**, the simulation has been compared with experimental data of two InAs-rich SL pin photodiodes having a cut-off wavelength of 5.35 µm (sample A) and 5 µm (sample B) measured by *Giard et al.* [**25**]. The energy band gap difference observed is due to a slight variation in the composition and thickness of the SL period between both samples. However, it has been demonstrated that this doesn't affect the material parameters used for the simulation [**14**]. At a wavelength of 4.5 µm (close to the cut-off wavelength), the calculated QE is 10 and 30% for sample A and B, respectively. These values are in good agreement with the measured values [**25**] demonstrating the model accuracy. The corresponding minority carrier diffusion length of the p-type InAs-rich SL has then been estimated to be slightly inferior to 4 µm at 77K. An absorption thickness of 4 µm has therefore been defined to optimize the quantum efficiency. Note that, at temperatures higher than 77K, the diffusion length is expected to be lower as the minority carrier lifetime and mobility decrease when the temperature increases.

The diffusion current is inversely proportional to the $N \times \tau$ product, with N the doping level of the active layer and τ the minority carrier lifetime. To reduce the diffusion current, the $N \times \tau$ product has thus to be maximise. According to reference [**26**], the optimum doping level for MWIR T2SL with a carrier lifetime of 100 ns is 2 x 10^{16} cm^{-3}. For this study, the doping level has been chosen to be close to the optimal value and it is equal to 1 x 10^{16} cm^{-3}.

2.2 Barrier layer

A variety of configurations is possible for the barrier structure depending on whether the active zone is n or p-type and if the contact layer is composed of the same material as the absorption region or not [**27**]. In our case, we will consider in this section that the contact layer is the same than the absorption region which is a p-type InAs-rich SL, in other words we will consider a *pBp* structure (inset **Figure 2**). In this configuration, the majority holes must be blocked by the barrier layer.

2.2a Band offset requirements

The majority holes coming from the contact layer can reach the absorption region by thermionic emission. In order to have a negligible effect of this current compared to the diffusion current, a large valence band offset between the absorption region and the barrier layer is required. To determine the valence band offset, we have calculated the thermionic current according to the analytic equation (3) [**28**].

$$J_{th}(\Delta E_v) = AT^2 e^{-\frac{\phi(\Delta E_v)}{kT}} \tag{3}$$

with

$$\phi = \Delta E_v + E_{fp}$$

and

$$A = \frac{4\pi q m_h^* k^2}{h^3}$$

where h is the Planck constant, ΔE_v is the valence band offset between the absorption region and the barrier layer and A is the Richardson constant which depends on the hole effective mass m_h^* and the extrinsic Fermi level E_{fp}.

The thermionic current variation with the valence band offset at a chosen temperature of 150K is plotted in **Figure 2**. To give us an idea of the required minimum valence band offset, we compared this current with the calculated diffusion current at 150K of an InAs-rich SL pin photodiode with an absorption

thickness of 4 µm and a p-type doping level of 1 x 10^{16} cm^{-3}. At -50 mV, the diffusion current calculated using the models and method given in reference [**14**] is equal to 4 x 10^{-4} A/cm^2. The thermionic current is equal to the diffusion dark-current for a valence band offset of 215 meV. Considering that the electric field is confined in the barrier, and so the depletion region, the potential drop will first happen in the barrier when a reverse bias is applied. If ΔE_v is not large enough, i.e. at its minimum value or less, the effective thickness of the potential barrier won't be sufficient anymore to block the majority holes. Thus, a larger valence band offset than 215 meV is needed. A value of 250 meV has been chosen for ΔE_v as for this value the thermionic contribution is lower by one order of magnitude than the diffusion dark-current.

On the other hand, the photogenerated electron carriers must reach the contact to be collected. The conduction band offset ΔE_c between the barrier and the absorption region when positive determines the device operating voltage. Indeed, if ΔE_c is large, a high reverse applied bias will be required to reduce the barrier in the conduction band. In order to allow the minority carrier flow, the conduction band offset has to be smaller than $3kT$, *i.e.* 38 meV for a temperature of 150K. The material for the barrier will be chosen to have no conduction band offset and a valence band offset of 250 meV with the InAs-rich SL in **section 2.2d**.

2.2b Barrier thickness

In addition to the thermionic emission, the majority holes can tunnel from the contact to the absorption region through the barrier. This tunnelling current, which depends on the barrier thickness and the valence band offset ΔE_v, has been calculated using the method established by *Klipstein et al.* [**28**]. In **Figure 3**, the tunnelling current is plotted as a function of the barrier thickness for a valence band offset of 250 meV at 150K. We also reported in **Figure 3** the diffusion dark-current of the InAs-SL pin photodiode as reference. It can be seen that for a barrier thickness of 62 nm, the tunnelling contribution

is equal to the diffusion current. However, to avoid the quick spreading of the electric field in the absorption region with the reversed applied bias, the barrier layer cannot be too thin.

Even though we can see from **Figure 3** that 100 nm is largely enough to have a negligible effect of the tunnelling current (more than 4 orders of magnitude compared to the diffusion current), a thickness of 200 nm has been chosen to ensure that the G-R current will appear at larger reverse bias that it would have been with 62 nm or 100 nm for example.

Furthermore, it is worth mentioning that in our configuration (*i.e.* large band offset in the valence band), the material composing the barrier is generally based on a superlattice material that is lattice matched to the GaSb substrate [**9, 11**]. Therefore, there is *a priori* no critical thickness for the barrier layer.

2.2c Barrier doping

Before investigating the influence of the barrier doping level on the electro-optical performances, we have studied the effect of the barrier doping type, whether n or p with a doping level of 1 x 10^{16} cm^{-3}, on the energy band diagram at 0 V (**Figure 4a and 4b**).

When the barrier is n-type and the absorption region p-type a pn junction is created at the interfaces between both. The majority electrons in the barrier and the majority holes in the absorption region diffuse and recombine until the equilibrium is reached and that the carrier diffusion is compensated by the electric field. Thereby, since the barrier thickness is relatively small, the barrier is fully depleted, so that the depletion region is extending into the absorption region on the right side of the barrier as illustrated in **Figure 4a**. To avoid the G-R current started from 0 V arising from the depletion region in the narrow band gap material, the 200 nm thick barrier layer cannot be n-type when the active zone is p-type.

In **Figure 4b**, the energy band diagram is plotted for a p-type barrier. In this case, the majority holes in the barrier diffuse to the absorption region and accumulate at the interfaces between both. As

previously, the barrier is fully depleted given its thickness. However, thanks to the narrow accumulation zone in the absorption layer, the electric field remains confined into the barrier, and so the depletion region. If a reverse bias is applied, this accumulation zone will tend to disappear and at a certain voltage, the depletion region will extend to the absorption layer creating a G-R current. The applied bias at which it will happen mainly depends on the thickness and doping level of the barrier layer.

The quantum efficiency at 4.5 µm and the dark-current density have been calculated as a function of the applied bias for different p-type doping levels of the 200 nm thick barrier layer at 150K. Results are presented in **Figure 5a and 5b** considering a p-type contact layer.

For a doping level of 5 x 10^{16} cm^{-3}, the potential barrier in the conduction band is extremely large of about 356 meV. Consequently, the photogenerated carriers cannot reach the contact and be collected for small reverse biases. This generates a really low dark-current density but also an extremely low quantum efficiency. In contrast, for doping levels below 5 x 10^{15} cm^{-3}, the potential barrier in the conduction band is only slightly superior to $3kT$, the quantum efficiency at 4.5 µm is therefore almost equal to the maximum quantum efficiency. For a doping level of 1 x 10^{16} cm^{-3} as the absorption region, the potential barrier in the conduction band is close to 84 meV, a small reverse voltage is therefore required to allow the carrier to be collected.

We can observe in **Figure 5b** that the dark-current is increasing at higher applied voltage. This behaviour is directly related to the extension of the depletion region in the absorption region and the apparition of the G-R current. For low doping levels, the G-R current appears at smaller reverse bias as there is less holes that accumulate at the interfaces between the barrier and the absorption region.

In conclusion, we have demonstrated that a p-type doping level which does not exceed the doping level of the absorption region is required for the barrier layer in order to have a low operating voltage. As compromise between a low operating voltage and the apparition of the G-R current, the barrier doping level has been chosen to be equal to 1 x 10^{16} cm^{-3}.

2.2d Barrier composition

In the literature, two different SL material systems are generally reported as material for the barrier composing *nBp* and *pBp* structures, either the InAs/GaSb/AlSb/GaSb SL [**9, 29, 30**] or the InAs/AlSb SL [**11**]. We have chosen to study the InAs/GaSb/AlSb/GaSb SL as it offers more flexibility in the choice of the band offset thanks to the additional GaSb layer.

To determine the period composition and thickness of the InAs/GaSb/AlSb/GaSb SL that match the requirements given in **section 2.2a**, a modified envelope function approximation model has been used to calculate the energy band gap and band offset with the InAs-rich SL. This model which is also used for the InAs/GaSb SL, describes the interfaces between the InAs and GaSb layers with a short-range delta-function potential created at the interfaces [**31**].

In **Figure 6**, using material parameters deduced from InAs/AlSb/GaSb N-structure [**32**], the calculated valence and conduction band offsets at 77K between the InAs/GaSb/AlSb/GaSb and the InAs-rich SL are reported for different period compositions. Note that, in the case of SLs, the conduction band offset is defined as the energy difference between the bottom of the two electron mini-bands and the valence band offset as the energy difference between the top of the two hole mini-bands.

It can be seen that for an

InAs/GaSb/AlSb/GaSb SL period composed of 8/1/5/1 MLs, the calculated valence band offset is slightly superior to 250 meV (**Figure 6a**) and there is no conduction band offset (**Figure 6b**) with the InAs-rich SL. Assuming that both SL material systems have a similar variation of the energy band gap with the temperature, we can consider that these band offset values will be the same whatever the temperature. Consequently, the 8 MLs InAs/1 ML GaSb/5 MLs AlSb/1 ML GaSb SL has been chosen as the material for the barrier layer.

2.3 Contact layer

In a barrier structure, the material for the contact layer can be different or not from the absorption region. For this work, we chose a similar material which is the InAs-rich SL for both the contact and the absorber.

Concerning the thickness of the contact layer, it is not as critical as the barrier thickness. However, it cannot be too thick to not penalize the quantum efficiency by absorbing some of the incident light. Typically, a thickness between 100 and 200 nm can be used for the contact layer.

In **Figure 7**, the energy band diagram of a *nBp* and *pBp* structures are compared for an equivalent contact doping level of 1 x 10^{16} cm^{-3} at T= 150K. For a *nBp* structure, the conduction band in the contact layer is close to the Fermi level, the thermionic current is therefore smaller since the potential barrier in the valence band is larger on the left side of the barrier. We can also observe that an n-type contact allows decreasing the potential barrier in the conduction band thus reducing the device operating voltage compared to a *pBp* device. On the other hand, less holes accumulate at the interface between the barrier and the absorber layer. The G-R current will therefore appear at a smaller voltage for an n-type contact. For a p-type barrier with a doping level of 1 x 10^{16} cm^{-3}, a n-type contact doping level of 1 x 10^{16} cm^{-3} can be chosen as there is still the narrow hole accumulation layer in the absorption region to confine the electric field into the barrier layer, as illustrated in **Figure 7**.

3- Dark-current performance of MWIR T2SL *nBp* device

Figure 8 presents the optimized MWIR T2SL *nBp* structure on GaSb substrate in terms of composition, thickness and doping level, along with the corresponding energy band diagram at a temperature of 150K and at 0 V. To ensure an ohmic contact, the top contact layer is also composed of 60 nm thick N^+ doped InAs-rich SL and 20 thick N^+ doped InAs cap layer.

Figure 9 displays the calculated dark-current density at -50 mV of the *nBp* device as a function of the temperature. For sake of comparison, the electrical performances of the equivalent pin photodiode, with the same absorber region as the *nBp* structure (InAs-rich SL with the 7MLs InAs/4MLs GaSb period [14]), is also plotted in addition to the variation of the G-R and diffusion contributions. In **Figure 9**, J_{ph} denotes the calculated photonic current at f/2 for a quantum efficiency close to the cut-off wavelength of 47%, which is the estimated value considering an antireflection coating. J_{obs} has been defined as the dark-current required to achieve high performance, *i.e.* value at which it does not degrade the performances. It has a value usually taken as two order of magnitude lower than J_{ph}.

The crossing temperature (T_c) between the G-R and diffusion regime of the pin photodiode is close to 136K. The G-R current being suppressed at small applied bias, the *nBp* structure is, as expected, limited by the diffusion current at -50 mV on the overall range of temperature. Above T_c, the *nBp* device doesn't permit to significantly improve the dark-current compared to the pin photodiode since the latter is also diffusion-limited. At a temperature of 150K, the dark current of the *nBp* device is equal to 1.5 x 10^{-4} A/cm^2 which is lower by a factor of 2.6 than the pin photodiode. This value is within two decades compared to values from the well-known 'rule 07' [**33**] showing the difficulties of the T2SL technology to reach similar dark-current performances than Mercury Cadmium Telluride (MCT or HgCdTe) detectors in the MWIR domain. This is directly attributable to the short minority carrier lifetime in the T2SL material. Nevertheless, below T_c, the improvement in terms of dark-current or operating temperature is considerable compared to the standard pin photodiode. Indeed, at 77K, we can expect with the *nBp*

device a decrease of three orders of magnitude for the dark-current compared to the pin photodiode that has a dark-current level of 1 x 10^{-8} A/cm^2. Furthermore, at iso-performance for a current density equal to J_{obs} = 5.8 x 10^{-7} A/cm^2, the operating temperature of the pin photodiode is close to 100K while for the *nBp* structure it is 120K. An improvement of 20K on the operating temperature is considerable as it determines the power consumption and the cool-down time of the cooled IR system. According to *Manissadjian et al.* [**34**] an improvement of 30K can lead to a decrease by a factor of two on the power consumption which will directly have an impact on the *SWaP* (Size, Weight and Power) criteria.

In conclusion, depending on the application, *i.e.* field of view, scene temperature, etc., the barrier structure will allow improving the performances over the standard pin photodiode in the MWIR spectral domain. In addition, barrier structures can be used to overcome passivation issues thanks to the presence of the barrier layer covering the absorption region [**7**]. This can be interesting for smaller energy band gap (LWIR) since the surface leakage, that may appear, is more significant as it is associated with surface states within the band gap and the pinning of the Fermi level. In the next section, preliminary results using the *nBp* structure for the LWIR are presented and discussed for a temperature of 77K.

4- *nBp* structure for the long-IR spectral domain

Since the energy band gap of T2SL is determined by the period composition and thickness, which can be precisely controlled during the growth by molecular beam epitaxy, high uniformity in terms of material properties and electro-optical performances can be achieved on GaSb substrate [**35**]. This is a considerable advantage over the MCT technology as the performances are degraded at longer wavelength due to inherent compositional nonuniformity at lower CdTe mole fraction of the alloy required to access this spectral domain. It is therefore essential to evaluate the performances and the potentiality of the T2SL technology for the LWIR domain.

As material for the absorption region, we chose the T2SL composed of 14 MLs of InAs and 5MLs of GaSb (14/5) that has a cut-off wavelength of 12 µm at 77K, which has been calculated using the model previously described in **section 2.2d**. The material parameters used for the simulation summarized in **Table 2** are in part extracted from reference [**15**]. The minority carrier lifetime has been set equal to 30 ns as it is the typical value measured for LWIR T2SL [**21**].

The material for the barrier has been defined using the same previous method. The InAs/GaSb/AlSb/GaSb SL composed of 12/1/5/1 MLs has been found to have no conduction band offset and a valence band offset of 340 meV with the 14/5 T2SL.

As a first attempt, the exact same *nBp* structure than the one reported in **Figure 8** has been used. However, due to a larger potential barrier in the conduction band than in the MWIR domain caused by a smaller energy band gap and the barrier doping level, the barrier doping level has been decreased to 5 x 10^{15} cm^{-3}. The energy band diagram of the *nBp* LWIR structure is presented in **Figure 10** along with the energy band diagram of the equivalent pin photodiode with the same absorption region.

The simulated dark-current density at 77K of the LWIR *nBp* structure and the pin photodiode is plotted in **Figure 11**. On one hand, it can be observed that the pin photodiode is limited by the G-R current at small reverse bias with a dark-current level of 5.7 x 10^{-3} A/cm^2 at -50 mV. Starting from -120 mV, the band-to-

band tunnelling current (BTB) appears to be the main contribution to the dark-current. The energy band gap being smaller in this spectral range, the tunnelling contribution dominates at smaller voltage than in the MWIR domain. On the other hand, as expected, the LWIR *nBp* device is limited by the diffusion current up to -0.3 V with a flat dark-current level of 3.5 x 10^{-4} A/cm^2 which is more than one order of magnitude lower compared to the performance of the pin photodiode. This result is at the state of the art compared to the well-known MCT 'rule 07' [**33**] demonstrating that InAs/GaSb SL detectors can be a serious competitor to the MCT technology at longer wavelength. This can be explained by the fact that even though the minority carrier lifetime in the T2SL material is lower than in the MCT, the $N \times \tau$ product is maximum for a lower doping level in the MCT [**26**]. Therefore, the short minority carrier lifetime in the T2SL can be compensated by choosing a higher doping level. In addition, the T2SL technology benefits from a high operability of focal plane arrays with very few flickering pixels [**36**] and an image stability with no deterioration of the image quality over time.

5 – Conclusion

Using the commercial TCAD ATLAS software from SILVACO, each layer of the barrier device has been optimized in terms of composition, doping and thickness by analysing energy band diagrams and the electro-optical performances. The proposed *nBp* device addressing the MWIR spectral domain is made of a 4 µm thick p-type (1 x 10^{16} cm^{-3}) InAs-rich SL absorption region, a 200 nm thick p-type (1 x 10^{16} cm^{-3}) InAs/GaSb/AlSb/GaSb high band gap SL barrier and an n-type (1 x 10^{16} cm^{-3}) InAs-rich SL contact layer. The electrical performances of this structure have been evaluated and compared to the equivalent pin photodiode having the same absorption region.

As expected, the MWIR *nBp* device is limited by the diffusion current on the overall range of temperature from 77 up to 200K whereas the pin photodiode is limited by the G-R current below a temperature of 136K. Since the pin photodiode is diffusion limited at high temperatures (> 136K), the dark-current at 150K of the MWIR *nBp* device is lower by only a factor of 2.6 with a dark-current level of 1.5 x 10^{-4} A/cm^2. Even though this value is higher than the dark-current of MCT detectors due to the short minority carrier lifetime in the T2SL material, the improvement at low temperatures is considerable compared to the pin photodiode. We have demonstrated that at 77K the dark-current level of the MWIR *nBp* device is three orders of magnitude lower than the pin photodiode and that for the defined J_{ph} at f/2 with the estimated QE of 47%, the MWIR *nBp* device can operate to a temperature up to 120K resulting in an improvement of 20K on the operating temperature.

Using the same *nBp* structure with a lower p-type doping level (5 x 10^{15} cm^{-3}) for the barrier layer, the electrical performance of LWIR T2SL device has been simulated. At 77K, the LWIR T2SL barrier detector is limited by the diffusion current up to – 0.3V with a flat current density of 3.5 x 10^{-4} A/cm^2 which is more than one order of magnitude lower compared to pin photodiode. This result is at the state of the art compared to the well-known MCT 'rule 07' demonstrating that InAs/GaSb SL detectors can be a serious competitor to the MCT technology in the LWIR domain, considering also that MCT detector suffers from

compositional nonuniformity at longer wavelength. The fabrication and characterizations of LWIR T2SL barrier detectors will be the subject of further investigation to confirm such simulation results.

References

[1] D.L. Smith and C. Mailhiot, J. Appl. Phys **62** (1987) 2545.

[2] E. H. Steenbergen, G. Ariyawansa, C. J. Reyner, G. D. Jenkins, C. P. Morath, J. M. Duran, J. E. Scheihing, and V. M. Cowan, Proc. of SPIE **10111** (2017) 1011104-1.

[3] B. V. Olson, E. A. Shaner, J. K. Kim, J. F. Klem, S. D. Hawkins, L. M. Murray, J. P. Prineas, M. E. Flatté, and T. F. Boggess, Appl. Phys. Lett. **101** (2012) 092109.

[4] E. H. Steenbergen, B. C. Connelly, G. D. Metcalfe, H. Shen, M. Wraback, D. Lubyshev, Y. Qiu, J. M. Fastenau, A. W. K. Liu, S. Elhamri, O. O. Cellek, and Y.-H. Zhang, Appl. Phys. Lett. **99** (2011) 251110.

[5] T. Schuler-Sandy, S. Myers, B. Klein, N. Gautam, P. Ahirwar, Z.-B. Tian, T. Rotter, G. Balakrishnan, E. Plis, and S. Krishna, Appl. Phys. Lett. **101** (2012) 071111.

[6] P.C. Klipstein, Y. Livneh, A. Glozman, S. Grossman, O. Klin, N. Snapi, and E. Weiss, J. Electron. Mater. **43** (2014) 2984.

[7] S. Maimon and G.W. Wicks, Appl. Phys. Lett. **89** (2006) 151109.

[8] J.B. Rodriguez, E. Plis, G. Bishop, Y.D. Sharma, H. Kim, L.R. Dawson, S. Krishna, Appl. Phys. Lett. **91** (2007) 043514.

[9] S. Abdollahi Pour, E. K. Huang, G. Chen, a. Haddadi, B.-M. Nguyen, and M. Razeghi, Appl. Phys. Lett. **98** (2011) 143501.

[10] D.Z. Ting, C.J. Hill, A. Soibel, S.A. Keo, J.M. Mumolo, J. Nguyen, S.D. Gunapala, Appl. Phys. Lett. **95** (2009) 023508.

[11] P.C. Klipstein, E. Avnon, Y. Benny, R. Fraenkel, A. Glozman, S. Grossman, O. Klin, L. Langoff, Y. Livneh, I. Lukomsky, M. Nitzani, L. Shkedy, I. Shtrichman, N. Snapi, A. Tuito, E. Weiss, Proc. SPIE **9070** (2014) 90700U-1.

[12] R. Taalat, J.B. Rodriguez, M. Delmas, P. Christol, J. Phys. D: Appl. Phys. **47** (2014) 015101.

[13] Silvaco ATLAS Users Manual, https://dynamic.silvaco.com/dynamicweb/jsp/downloads/DownloadManualsAction.do?req=silen-manuals&name=atlas

[14] M. Delmas, J.B. Rodriguez, P. Christol, J. Appl. Phys. **116** (2014) 113101.

[15] K. Banerjee, J. Huang, and S. Ghosh, Inf. Phys. Technol. **54** (2011) 460.

[16] J. Abautret, J.P. Perez, A. Evirgen, F. Martinez, P. Christol, J. Fleury, H. Sik, R. Cluzel, A. Ferron, Y. Rothman, J. Appl. Phys. **113** (2013) 183716.

[17] E. Giard, I. Ribet-Mohamed, J. Jaeck, T. Viale, R. Haïdar, R. Taalat, M. Delmas, J.B. Rodriguez, E. Steveler, N. Bardou, F. Boulard, P. Christol, J. Appl. Phys. **116** (2014) 043101.

[18] E. Steveler, M. Verdun, B. Portier, P. Chevalier, C. Dupuis, N. Bardou, J.B. Rodriguez, R. Haïdar, F. Pardo, J.L. Pelouard, Appl. Phys. Lett. **105** (2014) 141103.

[19] Z.B. Tian, E.A. Plis, R.T. Hinkey, S. Krishna, Electron. Lett. **50** (2014) 1733.

[20] S.P. Svensson, D. Donetsky, D. Wang, H. Hier, F.J. Crowne, G. Belenky, J. Cryst. Growth **334** (2011) 103.

[21] D. Donetsky, G. Belenky, S. Svensson, and S. Suchalkin, Appl. Phys. Lett. **97** (2010) 52108.

[22] F. Szmulowicz, S. Elhamri, H. J. Haugan, G. J. Brown, and W. C. Mitchel, J. Appl. Phys. **105**, (2009) 74303.

[23] C. Cervera, J. B. Rodriguez, J. P. Perez, H. Aït-Kaci, R. Chaghi, L. Konczewicz, S. Contreras, and P. Christol, J. Appl. Phys. **106** (2009) 33709.

[24] L. Bürkle, F. Fuchs, J. Schmitz, and W. Pletschen, Appl. Phys. Lett. **77** (2000) 1659–1661.

[25] E. Giard, I. Ribet-Mohamed, M. Delmas, J.B. Rodriguez, P. Christol, Inf. Phys. Technol. **70** (2015) 103.

[26] M. Kopytko and A. Rogalski, Prog. Quantum Electron. **47** (2016) 1–18.

[27] P.C. Klipstein, O. Klin, S. Grossman, N. Snapi, I. Lukomsky, M. Yassen, D. Aronov, E. Berkowicz, A. Glozman, O. Magen, I. Strichman, R. Frenkel, E. Weiss, Proc. SPIE **8268** (2012) 82680U.

[28] P. C. Klipstein, Proc. SPIE **6940** (2008) 69402U.

[29] B.M. Nguyen, G. Chen, A.M. Hoang, S. Abdollahi Pour, S. Bogdanov, M. Razeghi, Appl. Phys. Lett. **99** (2011) 033501.

[30] G. Chen, A. Haddadi, A. Hoang, R. Chevallier, M. Razeghi, Opt. Lett. **40** (2015) 45.

[31] J.B. Rodriguez, P. Christol, F. Chevrier, A. Joullié, Physica E **28** (2005) 128.

[32] M. Hostut, M. Alyoruk, T. Tansel, A. Kilic, R. Turan, A. Aydinli, Y. Ergun, Super. Micro. **79** (2015) 116.

[32] W. E. Tennant, *J. Electron. Mater*. **39** (2010) 1030–1035.

[33] A. Manissadjian, L. Rubaldo, Y. Rebeil, A. Kerlain, D. Brellier, and L. Mollard, Proc. Of SPIE **8353** (2012) 835334.

[34] B.M. Nguyen, G. Chen, M.A. Hoang, and M. Razeghi, IEEE J. Quantum Electron. **47** (2011), 686–690.

[35] J. Nghiem, J. Jaeck, E. Giard, M. Caes, J.-B. Rodriguez, P. Christol, R. Haidar, E. Costard, and I. Ribet-Mohamed, Proc of SPIE **10111** (2017) 101111D.

TABLE CAPTION

Table 1: Material parameters of the MWIR 7/4 InAs-rich SL structure.

Table 2: Parameter values of the LWIR 14/5 InAs/GaSb T2SL.

TABLES

Parameters	**Values**
Energy band gap at T = 0K	249 meV
Varshni parameter α	0.30 meV/K
Varshni parameter β	450 K
Permittivity	15.34 x ε_0
Electron affinity	4.73 eV
Electron effective mass	$m^*_e = 0.0254 \times m_0$
Hole effective mass	$m^*_h = 0.245 \times m_0$

Table 1

Parameters	**Values**
Energy band gap at T = 77K	0.103 eV
Permittivity	15.29 x ε_0
Electron affinity	4.76 eV
Electron effective mass	$m^*_e = 0.027 \times m_0$
Hole effective mass	$m^*_h = 0.4 \times m_0$
Minority carrier lifetime	τ = 30 ns

Table 2

FIGURE CAPTIONS

Fig. 1: Simulated quantum efficiency at 77K and 0V of p-type InAs-rich SL pin photodiodes with an absorption thickness of 500 nm (sample A) and 4 µm (sample B). The curves obtained are in good agreement with the experimental data reported in reference [25].

Fig. 2: Thermionic current as a function of the valence band offset $\boldsymbol{\Delta E_v}$ between the absorption region and the barrier at 150K. The calculated diffusion dark-current of a p-type InAs-rich-SL pin photodiode is also plotted. Inset shows the schematic band diagram of a *pBp* structure at 0 V.

Fig. 3: Tunnelling current through the barrier layer at 150K as a function of the barrier thickness for a valence band offset of 250 meV. The calculated diffusion dark-current of a p-type InAs-SL pin photodiode is also plotted as reference.

Fig. 4: Energy band diagram calculated at 150K and at 0V of a *pBp* structure with a 200 nm thick (a) n-type and (b) p-type barrier. The doping level of the barrier and absorption region is 1 x 10^{16} cm^{-3}. E_c, E_v and E_f are respectively the conduction band, the valence band and the Fermi level.

Fig. 5: Simulated electro-optical performances of a MWIR *pBp* structure with a 200 nm thick barrier layer: (a) quantum efficiency at 4.5 µm and (b) dark current density as a function of the voltage at 150K for different p-type doping levels.

Fig. 6: Valence (a) and conduction (b) band offsets at 77K between the InAs / GaSb (1 ML) / AlSb / GaSb (1 ML) SL and the InAs-rich SL as a function of the InAs layer thickness for different AlSb layer thicknesses.

Fig. 7: Energy band diagram of the MWIR nBp (continuous line) and pBp (dashed line) structures at 150K and at 0V. The barrier and absorber doping level is equal to 1 x 10^{16} cm^{-3}.

Fig. 8: (a) Optimized MWIR *nBp* structure based on the p-type InAs-rich SL and (b) the corresponding energy band diagram at 150K and at 0V.

Fig. 9: Simulated dark-current density at -50 mV of the MWIR *nBp* structure (stars) and the equivalent pin photodiode (squares) as a function of the temperature. The variation of the G-R current (black line) and the diffusion current (red line) is also reported. J_{ph} is the calculated photonic current at f/2 for an estimated QE of 47%. J_{obs} is the required dark-current level.

Fig. 10: Energy band diagram at 77K and 0V of (a) the LWIR *nBp* structure and (b) the equivalent pin photodiode having a cut-off wavelength of 12 μm.

Fig. 11: Simulated dark-current density at 77K as a function of the voltage of the LWIR *nBp* structure and the equivalent pin photodiode. The LWIR *nBp* device is diffusion limited up to -0.3 V.

FIGURES

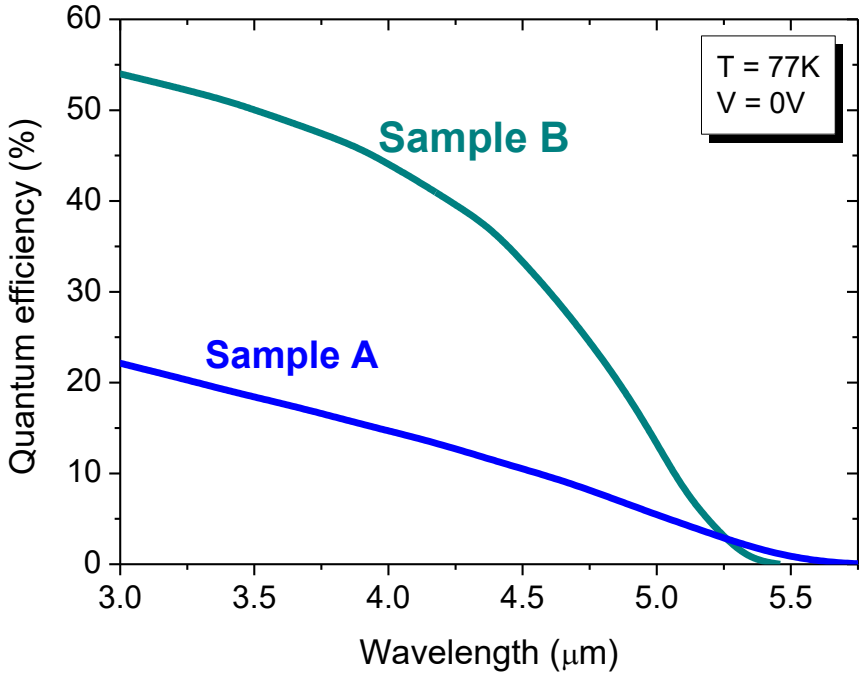

Figure 1.

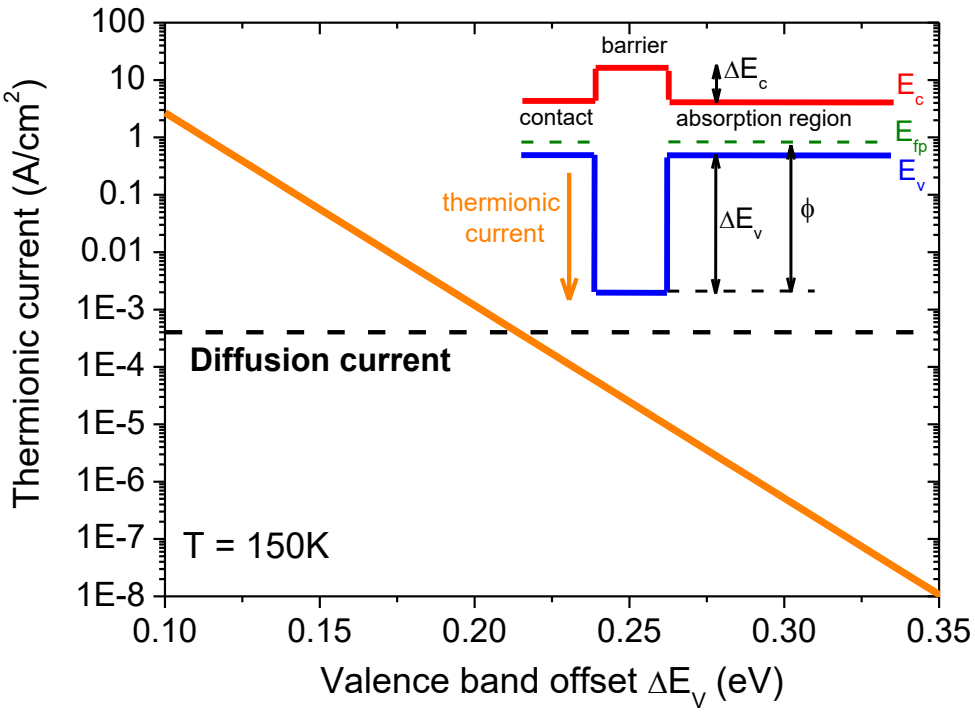
Thermionic current (A/cm^2)
100
10
1
0.1
0.01
1E-3
1E-4
1E-5
1E-6
1E-7
1E-8
0.10
0.15
0.20
0.25
0.30
0.35
Valence band offset ΔE_V (eV)
barrier
ΔE_c
E_c
contact
absorption region
E_{fp}
E_v
thermionic current
ΔE_v
ϕ
Diffusion current
T = 150K

Figure 2.

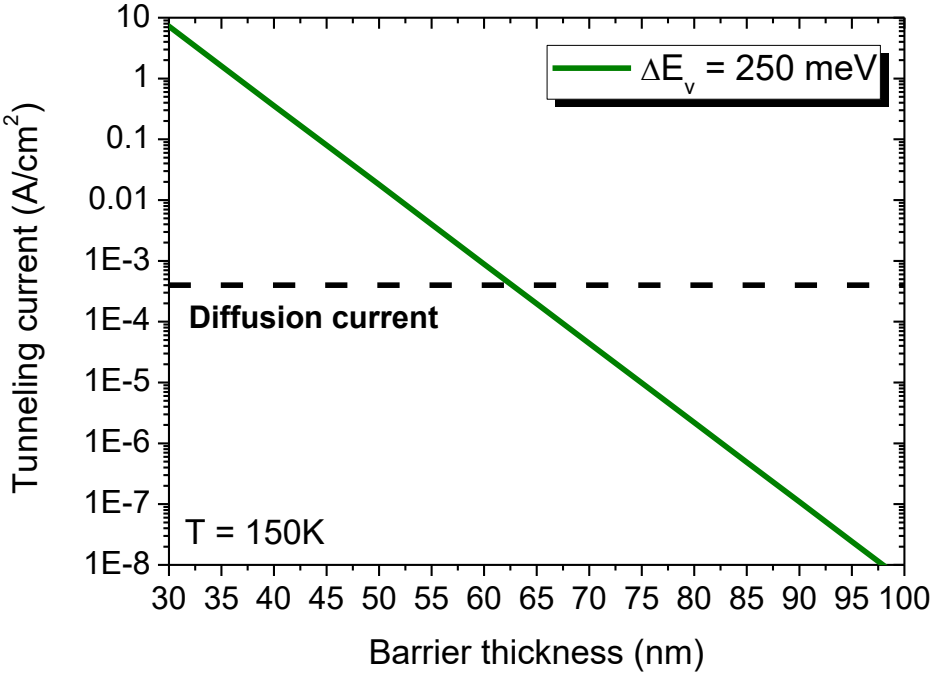
10
1
0.1
0.01
1E-3
1E-4
1E-5
1E-6
1E-7
1E-8
Tunneling current (A/cm^2)
30 35 40 45 50 55 60 65 70 75 80 85 90 95 100
Barrier thickness (nm)
ΔE_v = 250 meV
Diffusion current
T = 150K

Figure 3.

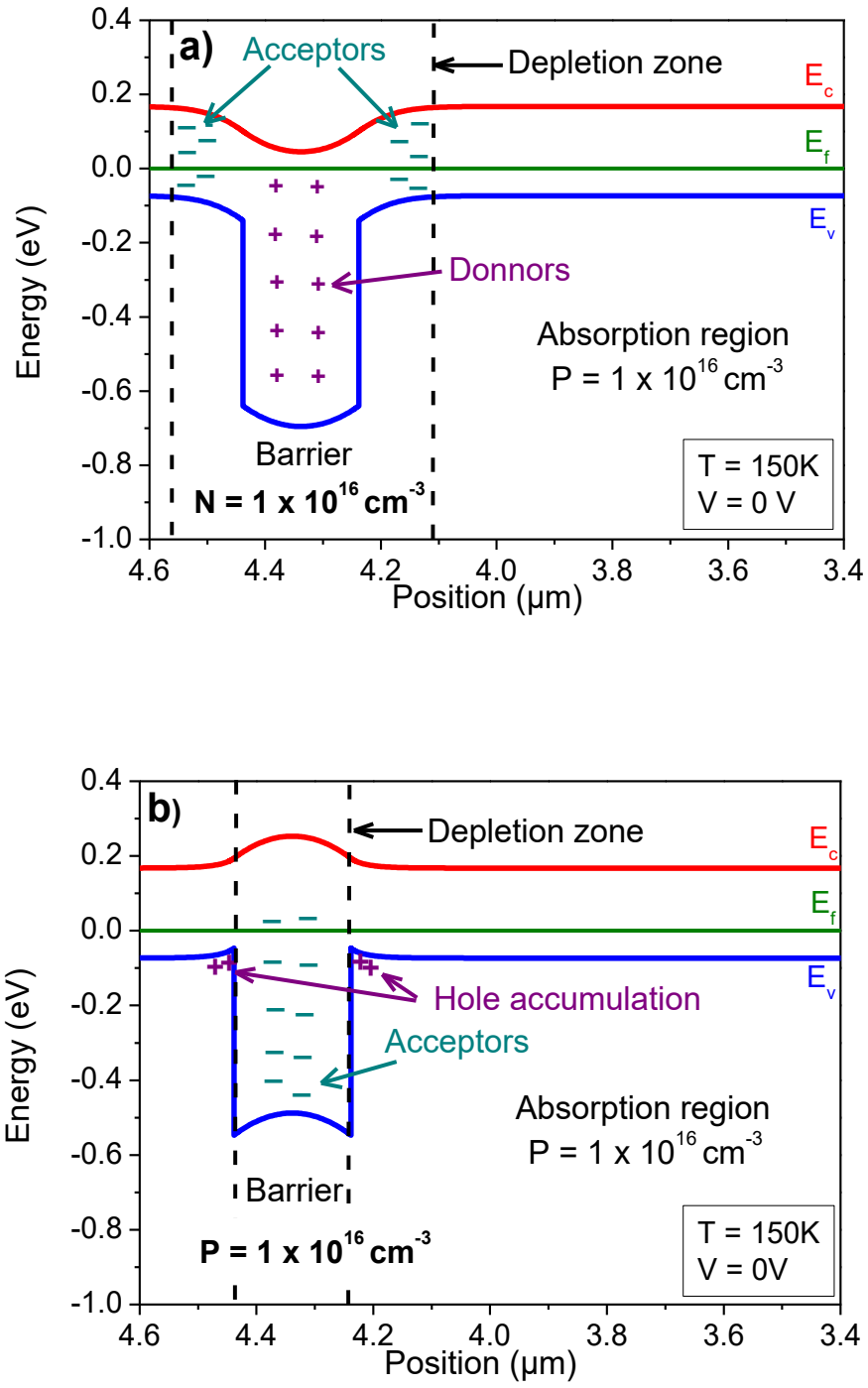
a)
Acceptors
Depletion zone
E_c
E_f
E_v
Donnors
Absorption region
P = 1 x 10^{16} cm^{-3}
Barrier
N = 1 x 10^{16} cm^{-3}
T = 150K
V = 0 V
Energy (eV)
Position (μm)
b)
Depletion zone
Hole accumulation
Acceptors
Absorption region
P = 1 x 10^{16} cm^{-3}
Barrier
P = 1 x 10^{16} cm^{-3}
T = 150K
V = 0V

Figures 4.

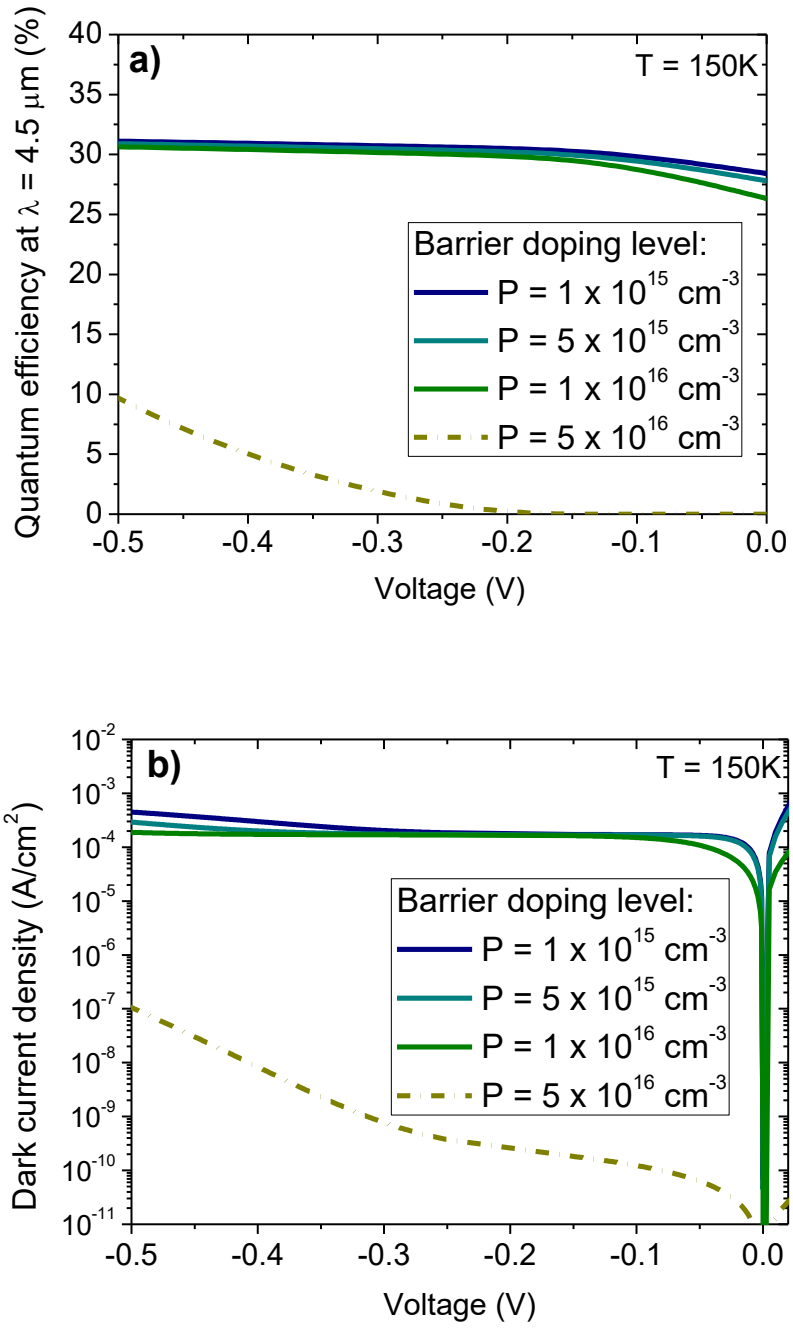
a)
T = 150K
Quantum efficiency at λ = 4.5 μm (%)
Voltage (V)
Barrier doping level:
P = 1 x 10^15 cm^-3
P = 5 x 10^15 cm^-3
P = 1 x 10^16 cm^-3
P = 5 x 10^16 cm^-3
b)
T = 150K
Dark current density (A/cm^2)
Voltage (V)
Barrier doping level:
P = 1 x 10^15 cm^-3
P = 5 x 10^15 cm^-3
P = 1 x 10^16 cm^-3
P = 5 x 10^16 cm^-3

Figures 5.

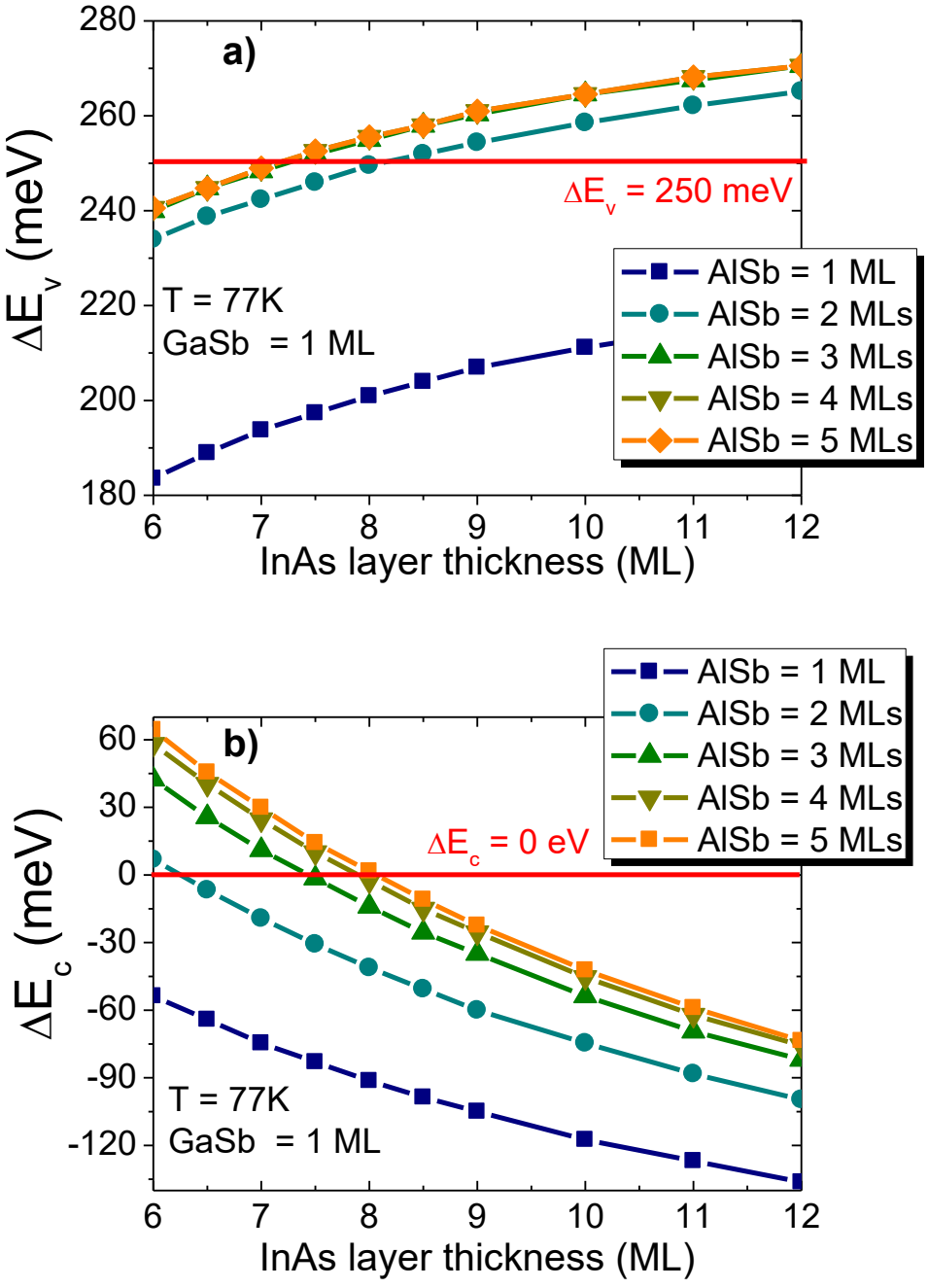
a)
ΔE_v = 250 meV
T = 77K
GaSb = 1 ML
AlSb = 1 ML
AlSb = 2 MLs
AlSb = 3 MLs
AlSb = 4 MLs
AlSb = 5 MLs
ΔE_v (meV)
InAs layer thickness (ML)
b)
ΔE_c = 0 eV
T = 77K
GaSb = 1 ML
ΔE_c (meV)
InAs layer thickness (ML)

Figures 6.

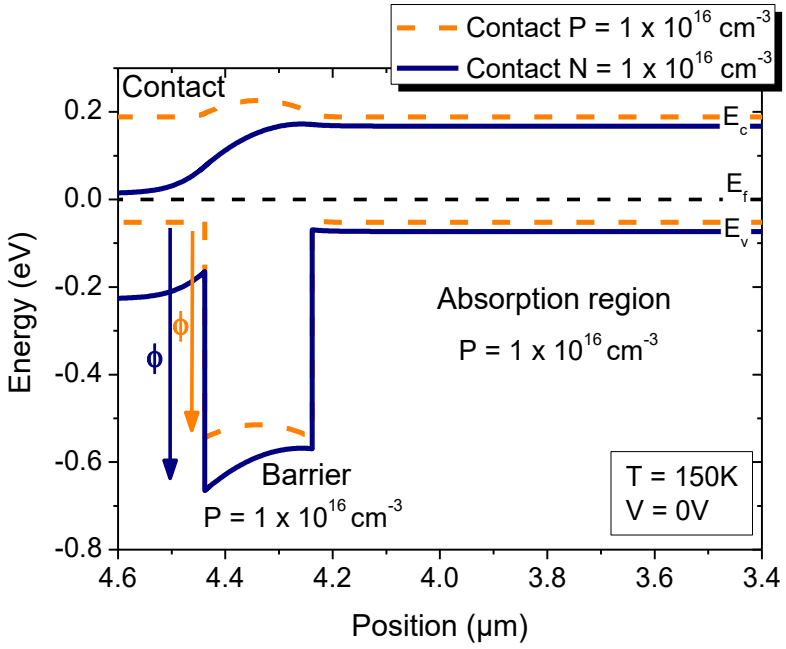
Contact P = 1 x 10^16 cm^-3
Contact N = 1 x 10^16 cm^-3
Contact
E_c
E_f
E_v
Absorption region
P = 1 x 10^16 cm^-3
Barrier
P = 1 x 10^16 cm^-3
T = 150K
V = 0V
ϕ
ϕ
Energy (eV)
Position (μm)
0.2
0.0
-0.2
-0.4
-0.6
-0.8
4.6
4.4
4.2
4.0
3.8
3.6
3.4

Figure 7.

(a)

Cap InAs	N ~ 5 x 10^{17} cm^{-3}	20 nm
InAs/GaSb SL (7/4 ML)	N ~ 5 x 10^{17} cm^{-3}	60 nm
CONTACT InAs/GaSb SL (7/4) **N ~ 1 x 10^{16} cm^{-3}** **140 nm**		
BARRIER InAs/GaSb/AlSb/GaSb SL (8/1/5/1 ML) **P ~ 1 x 10^{16} cm^{-3}** **200 nm**		
ACTIVE ZONE InAs/GaSb SL (7/4 ML) **P ~ 1 x 10^{16} cm^{-3}** **4 µm**		
InAs/GaSb SL (7/4 ML)	P ~ 5 x 10^{17} cm^{-3}	60 nm
GaSb Buffer	P ~ 5 x 10^{17} cm^{-3}	200 nm
GaSb substrate	Type P	

(b)

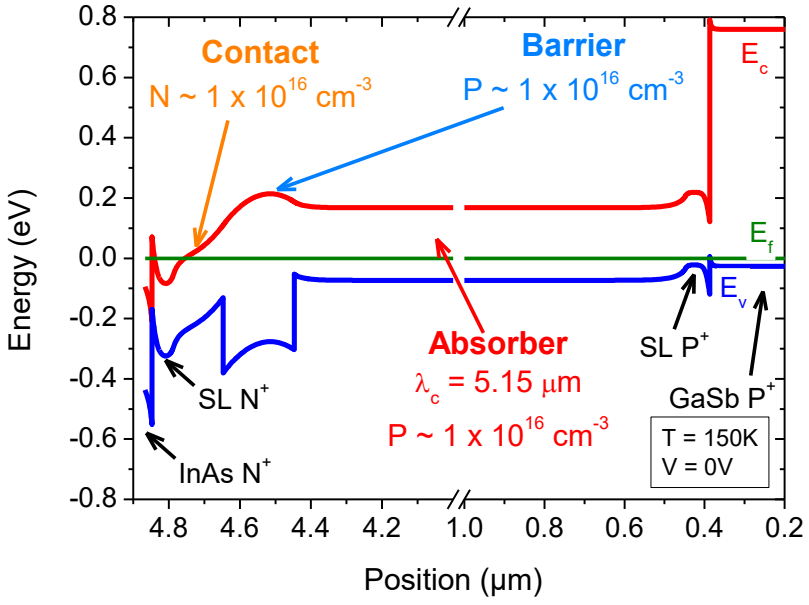

Figures 8.

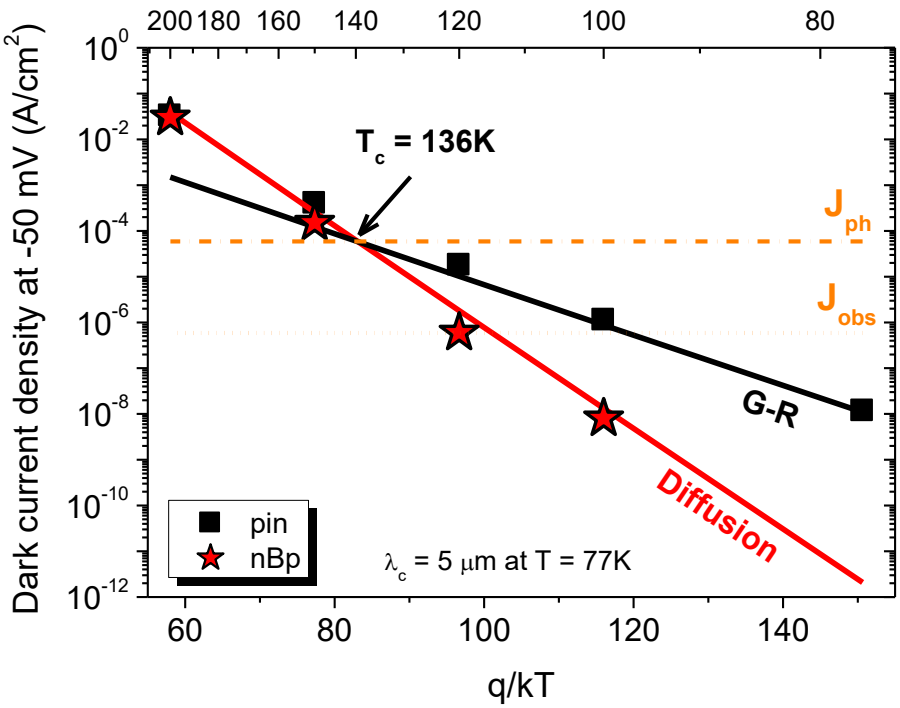
200 180 160 140 120 100 80
Dark current density at -50 mV (A/cm^2)
10^0
10^{-2}
10^{-4}
10^{-6}
10^{-8}
10^{-10}
10^{-12}
T_c = 136K
J_{ph}
J_{obs}
G-R
Diffusion
pin
nBp
λ_c = 5 μm at T = 77K
60 80 100 120 140
q/kT

Figure 9.

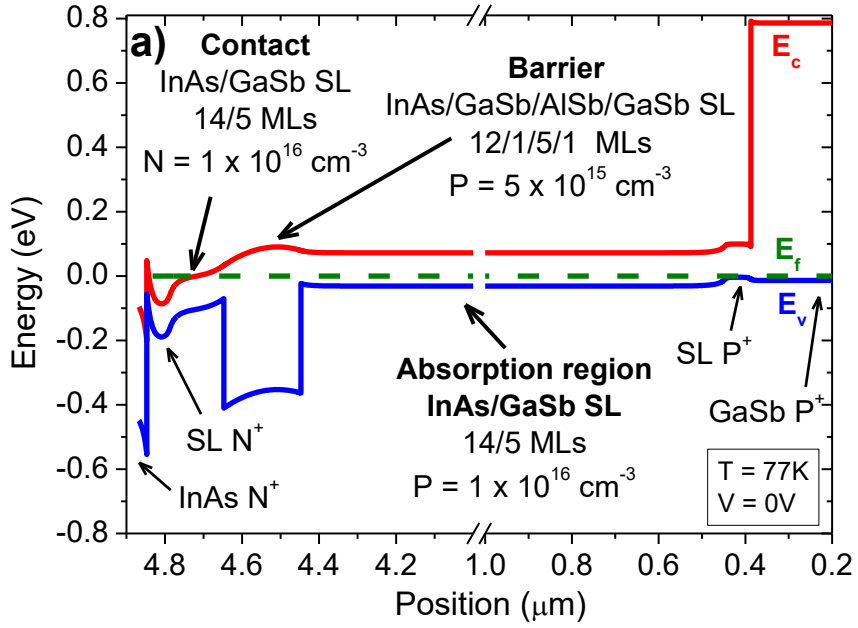
a)
Contact
InAs/GaSb SL
14/5 MLs
N = 1 x 10^16 cm^-3
Barrier
InAs/GaSb/AlSb/GaSb SL
12/1/5/1 MLs
P = 5 x 10^15 cm^-3
E_c
E_f
E_v
SL P+
GaSb P+
Absorption region
InAs/GaSb SL
14/5 MLs
P = 1 x 10^16 cm^-3
SL N+
InAs N+
T = 77K
V = 0V
Energy (eV)
Position (μm)

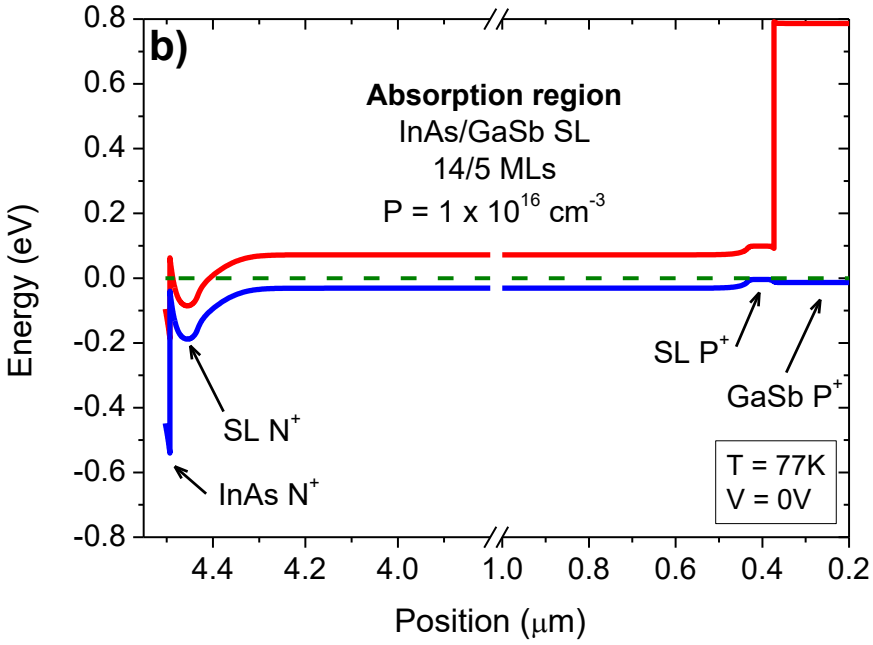
b)
Absorption region
InAs/GaSb SL
14/5 MLs
P = 1 x 10^16 cm^-3
SL P+
GaSb P+
SL N+
InAs N+
T = 77K
V = 0V
Energy (eV)
Position (μm)

Figures 10.

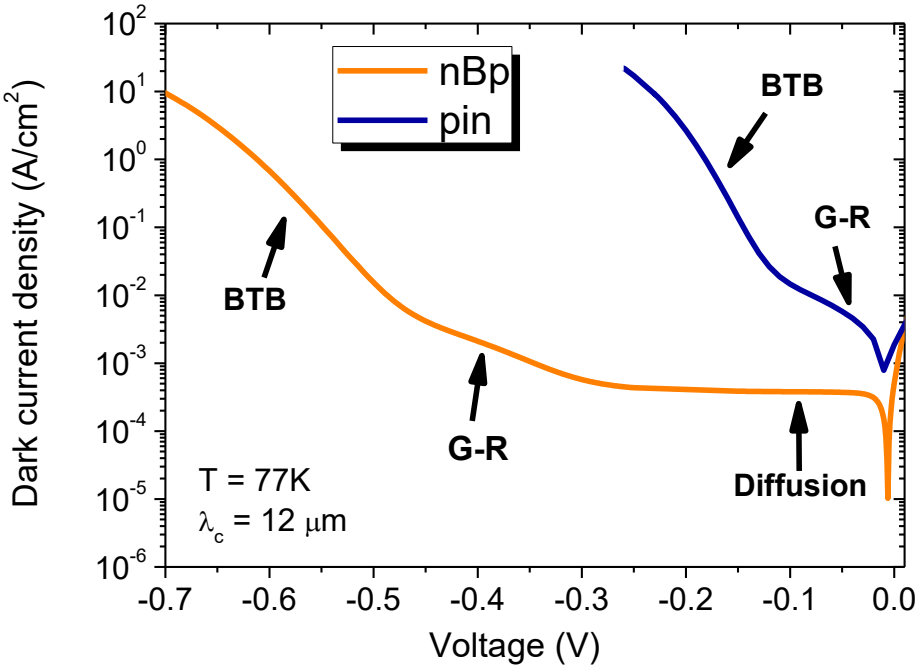
nBp
pin
BTB
G-R
BTB
G-R
Diffusion
T = 77K
λc = 12 μm
Dark current density (A/cm2)
Voltage (V)
10^2
10^1
10^0
10^-1
10^-2
10^-3
10^-4
10^-5
10^-6
-0.7
-0.6
-0.5
-0.4
-0.3
-0.2
-0.1
0.0

Figure 11.